PCCP

PAPER

View Article Online
View Journal | View Issue

Cite this: *Phys. Chem. Chem. Phys.*, 2025, **27**, 3420

High performance humidity sensor based on a graphene oxide–chitosan composite†

Parvesh Kumari,[abd] Ankit Kumar,[ad] Aditya Yadav,[cd] Ylias Sabri,[b] Samuel J. Ippolito,[b] Dilip. D. Shivagan[ad] and Komal Bapna *[ad]

Received 14th November 2024,
Accepted 2nd January 2025

DOI: 10.1039/d4cp04347b

rsc.li/pccp

In this study, we have proposed an advanced humidity sensor based on a composite of chitosan (CS) and graphene oxide (GO), prepared by the drop casting method. Graphene oxide–chitosan (GO–CS) films with varying volumetric ratios, along with pure GO and CS films, were prepared and extensively characterized using XRD, Raman, FTIR, SEM, XPS, and water contact angle to study their structural and morphological properties. Comparative analysis of humidity sensing parameters of all prepared films revealed that the film with a volumetric ratio of 4 : 1 (GOCS-2) performs best among all of them, which is attributed to the synergistic interaction between GO and CS. The optimized composite demonstrates high sensitivity, rapid response/recovery time, low hysteresis, and excellent repeatability as compared to pure GO and CS films. This study revealed that the enhanced performance is mainly driven by the increased hydrophilic functional groups and adsorption sites in the GO–CS composites. The optimized composite is proposed to be a promising candidate for the development of cost-effective and high-performance humidity sensors.

1. Introduction

Monitoring of relative humidity (RH) is increasingly essential across various sectors, including pharmaceuticals, agriculture, maintaining healthy, comfortable environmental conditions, and food storage sectors.[1,2] Consequently, the demand for accurate, affordable, and reliable RH sensors has become vital across consumer and industrial applications. These humidity sensors are mostly fabricated using various hygroscopic materials such as polymers, porous silicon, semiconductor metal oxides, or carbon-based materials.[1,3]

Graphene oxide (GO) is a derivative of graphene that contains oxygen functional groups (hydroxyl, epoxy, carbonyl, and carboxyl) attached to the sp^2 hybridized network of graphene sheets.[4,5] These functional groups make GO hydrophilic by providing a sensitive layer with a large number of active sites to adsorb water molecules.[6,7] Despite the large number of functional groups present in GO, the overlapping layered structure of GO limits the effective surface area available for humidity sensing and reduces the sensing performance. Thus, efforts have been made to increase the porosity and surface to volume ratio to increase sensitivity, response, and affinity toward water molecules. For example, H. Bi *et al.*[8] designed a capacitive based GO humidity sensor that reportedly exhibited ten times higher sensitivity than the best conventional humidity sensor, and X. Li *et al.*[9] demonstrated an enhanced sensitivity by integrating MWCNTs into GO film. Adding MWCNTs into a GO solution creates larger ripples and more holes, increasing the GO layer interplanar spacing and enhancing the physical adsorption of water molecules. Zhang *et al.* presented a high-performance humidity sensor based on a GO/Nafion/indium oxide nanocomposite, demonstrating ultrahigh sensitivity and outstanding stability.[10] Zhang *et al.* fabricated a SnS_2/GO nanocomposite and showed ultrafast response, negligible hysteresis, and superior performance compared to individual SnS_2 or GO sensors.[11] In another study, a high-performance self-powered humidity sensor was developed based on SnS_2/rGO nanohybrids, demonstrating fast response, wide sensing range, and good stability.[12] Thus, numerous studies have shown that forming composites with complementary materials can significantly enhance the humidity sensing performance of conventional GO.[13–18]

With this work, we studied the possibility to integrate CS polymer with GO film and their humidity sensing behavior. Polymers have attracted considerable interest in humidity sensing applications due to their straightforward synthesis

[a] *Temperature and Humidity Metrology, CSIR-National Physical Laboratory, Dr K. S. Krishnan Marg, New Delhi, 110012, India. E-mail: komal.bapna@nplindia.org*
[b] *Centre for Advanced Materials & Industrial Chemistry, School of Engineering, RMIT University, Melbourne, VIC, 3000, Australia*
[c] *Sensor Devices and Metrology, CSIR-National Physical Laboratory, Dr K. S. Krishnan Marg, New Delhi 110012, India*
[d] *Academy of Scientific & Innovative Research (AcSIR), Ghaziabad 201002, India*

† Electronic supplementary information (ESI) available: XPS survey scan for the synthesized materials and hysteresis curves for all the compositions. See DOI: https://doi.org/10.1039/d4cp04347b

and the ability to tailor functional groups to optimize water affinity.[19–21] Among the polymers, chitosan (CS) is a polysaccharide that occurs naturally, contains a high concentration of amino and hydroxyl functional groups in its molecular chain, and easily forms a gel when combined with GO.[22] Also, it is easy to functionalize, has excellent film-forming ability and low production cost, and is non-toxic.[23] Due to their excellent bio-compatibility properties, GO–CS composites have been used in various applications, including biomaterials, dye removal from water, and smart materials.[20,24] In the past few years, researchers have proposed that composites of CS with other hygroscopic materials have enhanced humidity sensing capabilities.[16,20,25]So, the large functional groups of GO–CS composite film may offer additional water-adsorption sites and improve humidity sensing properties.[26]

With this aim, we have focused our work on obtaining the optimized GO–CS composition for superior humidity sensing properties. A range of GO–CS composites were prepared with different GO and CS volumetric ratios, and the resulting sensors were evaluated for their sensitivity and response under varying humidity conditions. The hypothesis for the sensing mechanism has been proposed based on resistance variations in composites due to the adsorption/desorption of water vapor in different humidity environments. The innovative aspect of this work lies in the systematic optimization of GO–CS composites to address the limitations of GO-based sensors and achieve enhanced humidity sensing properties.

2. Materials and methods

Chemicals used

Graphite powder (99.999%, Alfa Aesar), potassium permanganate (99% $KMnO_4$, Sigma Aldrich), sulfuric acid (98% H_2SO_4), hydrogen peroxide (30% H_2O_2), hydrochloric acid (37% HCl), acetic acid (100%), ethanol (99.8%), and acetone (99.5%) from Merck, and CS (≥95% deacetylation, Sigma Aldrich) were used without any further purification.

Synthesis of GO

The modified Hummers' method was used for the synthesis of GO.[27] In short, firstly, 46 mL of concentrated H_2SO_4 was poured

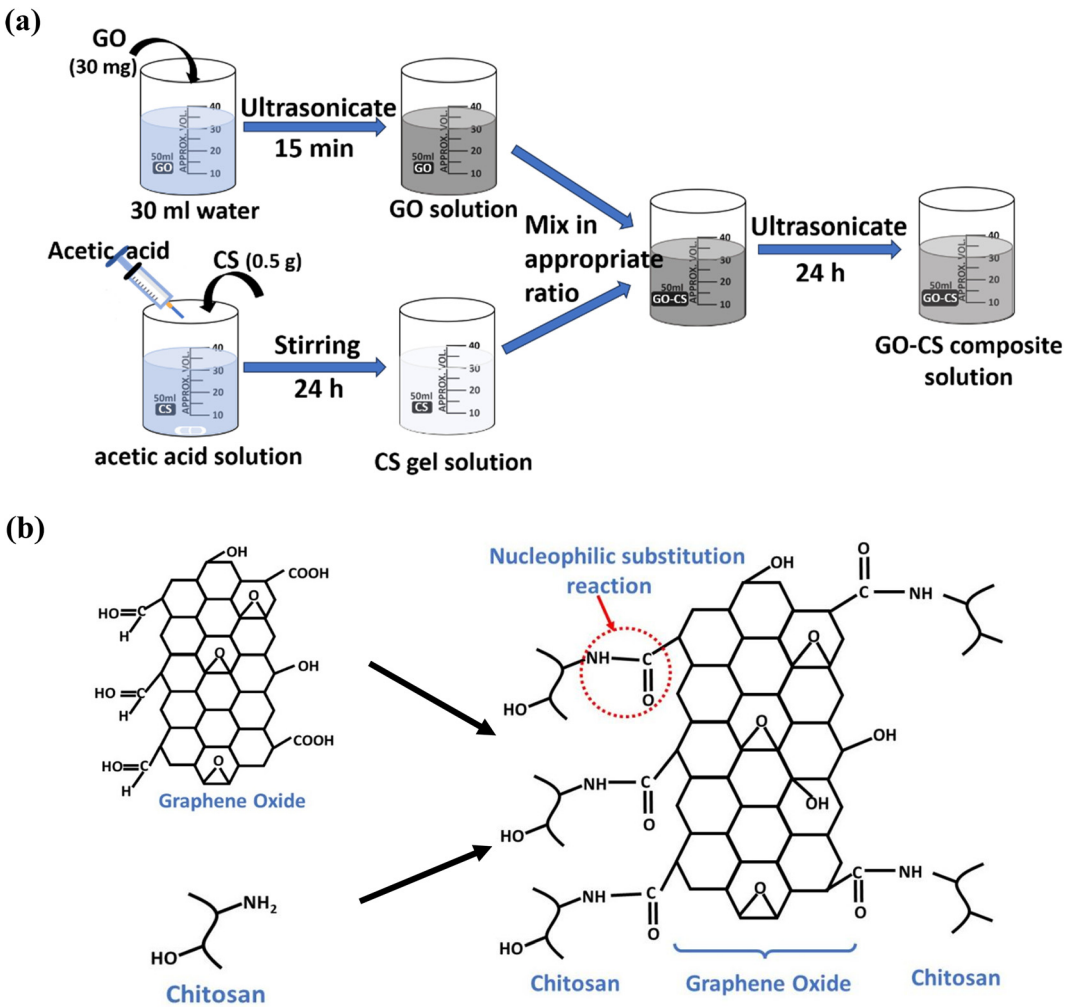

Fig. 1 (a) Flowchart for the synthesis procedure of the GOCS composites and (b) a chemical reaction schematic illustrating the process of amide bond formation between the GO and CS chain.

into a 500 ml flask with 2 g of graphite powder and vigorously stirred in an ice bath. After that, 6 g of $KMnO_4$ was added to the mixture with continuous stirring. Thereafter, 20 mL of H_2O_2 (30%) was added to the obtained mixture and stirred until the solution color changed into dark brown. To remove metal ions and neutralize the solution, the mixture was filtered and washed with HCl and DI water, then centrifuged several times until a neutral pH was obtained. The resulting dark brown sediment was dried in an oven at 60 °C for 1 h.

Preparation of GOCS composites

The GO–CS composites were synthesized *via* a facile solution mixing method.[28] For this, a homogenous suspension of GO (1 mg ml^{-1}) was added to the CS solution in different proportions. Initially, the CS solution was prepared by adding 0.5 g of CS powder to 100 ml of acetic acid (0.05 M) solution, as discussed in our previous work.[29] This resulted in a CS solution concentration of 5 mg ml^{-1}. Both the GO and CS solutions were mixed in an appropriate ratio and ultrasonicated for 1 h to form homogeneous suspensions followed by aging for 12 h at RT, as shown in Fig. 1(a). This results in the formation of amide covalent bonds due to the nucleophilic substitution reaction, between the carboxyl groups of GO and amine groups of CS, as depicted in Fig. 1(b).[30] To optimize the best configuration of GO–CS for humidity sensing, three GO–CS (v/v ratio) composites using different volumetric ratios, *i.e.*, GOCS-1 (1 : 1), GOCS-2 (4 : 1), and GOCS-3 (8 : 1) were prepared.

Fabrication of humidity sensors

To fabricate the humidity sensors, Ti/Au interdigitated electrodes (IDEs) with thickness 100/200 nm were deposited on a clean SiO_2/Si substrate (cleaned with acetone, isopropanol, and DI water), using an inter cross finger shadow mask with thickness (0.4 mm) by the DC sputtering technique. The pure and composite films were then deposited by dropping 20 μl of each on IDEs using a controlled micropipette and then dried at 60 °C for 20 min.

Measurements and experimental setup

XRD characterization of the GO, CS, and their composites was undertaken with a Rigaku Tabletop Miniflex-II using a monochromatic source $CuK_{\alpha 1}$ (λ = 1.5406 Å). The morphology and microstructure were examined using a TESCAN MAGNA GMH field-emission scanning electron microscope (FESEM). FTIR spectra were obtained with PerkinElmer Spectrum GX Fourier transform infrared spectroscopy. Raman spectra were measured using an inVia Raman Spectrophotometer (Renishaw) with a laser excitation wavelength of 532 nm. Different saturated salts *i.e.*, LiCl, KF, $Mg(NO_3)_2$, NaCl, KBr, and KNO_3, were used to generate various humidity environments of 11% RH, 33% RH, 52% RH, 75% RH, 85% RH, and 95% RH, respectively; see detailed discussed in our previous work.[29,31] A home-built dynamic gas sensing measurement setup with embedded probes was used to check selectivity over other gases.[32] A commercial hygrometer (testo 625, ±0.05% RH at 25 °C) was calibrated with the national primary standard to trace the RH of saturated salt solutions.

3. Results and discussion

Characterizations

The XRD patterns for the SiO_2/Si substrate, graphite, CS, GO, and GOCS-2 composite are shown in Fig. 2(a). Pure graphite shows a sharp and high intensity peak at 26.3° corresponding to the (002) plane with interlayer spacing (*d*-spacing) of 0.33 nm. After oxidation, the peak at 10.11° represents the (001) plane of GO with an increased *d*-spacing of 0.87 nm, indicating the oxygen-containing functional groups residing between graphite layers. The broad peak in the CS spectrum indicates its amorphous nature.[29] The broadening of the characteristic peaks of GO in the composite suggests CS incorporation between the GO layers, forming smaller crystallites while individual structures are intact. Furthermore, a slight peak shift towards lower angle is attributed to the increased GO layer spacing due to CS insertion, confirming the effective synthesis of composites, consistent with previous reports.[28,33]

The structural properties of each sample were characterized using Raman spectroscopy (Fig. 2(b)). In GO spectra, the G band at 1580 cm^{-1} corresponds to sp^2 carbon domains, and the D band at 1357 cm^{-1} is associated with the sp^3 carbon atom and disordered structures. The D and G peak intensity (I_D/I_G) ratio serves as a typical index for distinguishing between GO and composites with CS. The increase in I_D/I_G ratio of the composites is attributed to the enhanced sp^3 defects. The findings also accompany XRD results that show that the structural integrity of GO remains unaltered in the GO–CS composite. The dispersion of GO and CS in the composite was examined using SEM analysis (Fig. 2(c)–(f)). The surface of CS film is flat and relatively uniform in appearance,[29] while GO shows its typical wrinkled structure. In contrast, the GOCS-2 composite showed clumping and a less wrinkled surface than GO due to the gel like solution with incorporation of CS. Thus, the change in the morphology of the composite suggests that CS is incorporated into GO sheets. This finding is consistent with the previous reports, which show that CS molecules link nearby GO, thereby distributing the GO and CS throughout the composite.[28,30]

To better understand the molecular structures, FTIR spectra were examined, as illustrated in Fig. 3(a). The FTIR spectra of CS and GO are similar to our previous report,[23,30] while the spectrum of the composite showed characteristic peaks of CS and GO. Interestingly, the band at 1718 cm^{-1} for the GO sample was assigned to the carboxyl groups (C═O) and showed a clear downshift in GOCS-2 due to the hydrogen bonds between GO and CS. The band at 1631 cm^{-1} is attributed to epoxy groups and the C═C stretching of the sp^2 carbon network. The broad band at 3400 cm^{-1} indicates O–H & N–H bonds (C–O–H stretching), covalently bonded to carbon atoms.[28,29]

The XPS survey scan of GO shows two features at 284.6 (C1s) and 533 eV (O1s), while GOCS-2 spectra display an additional peak at 399.7 eV (N1s), as shown in ESI,† Fig. S1. The composite survey scan indicates an increase in oxygen and nitrogen levels, with an associated decrease in carbon content compared to GO. The high-resolution C1s spectra of the GOCS-2 composite (Fig. 3(b)) exhibit peaks corresponding to C–C or C═C

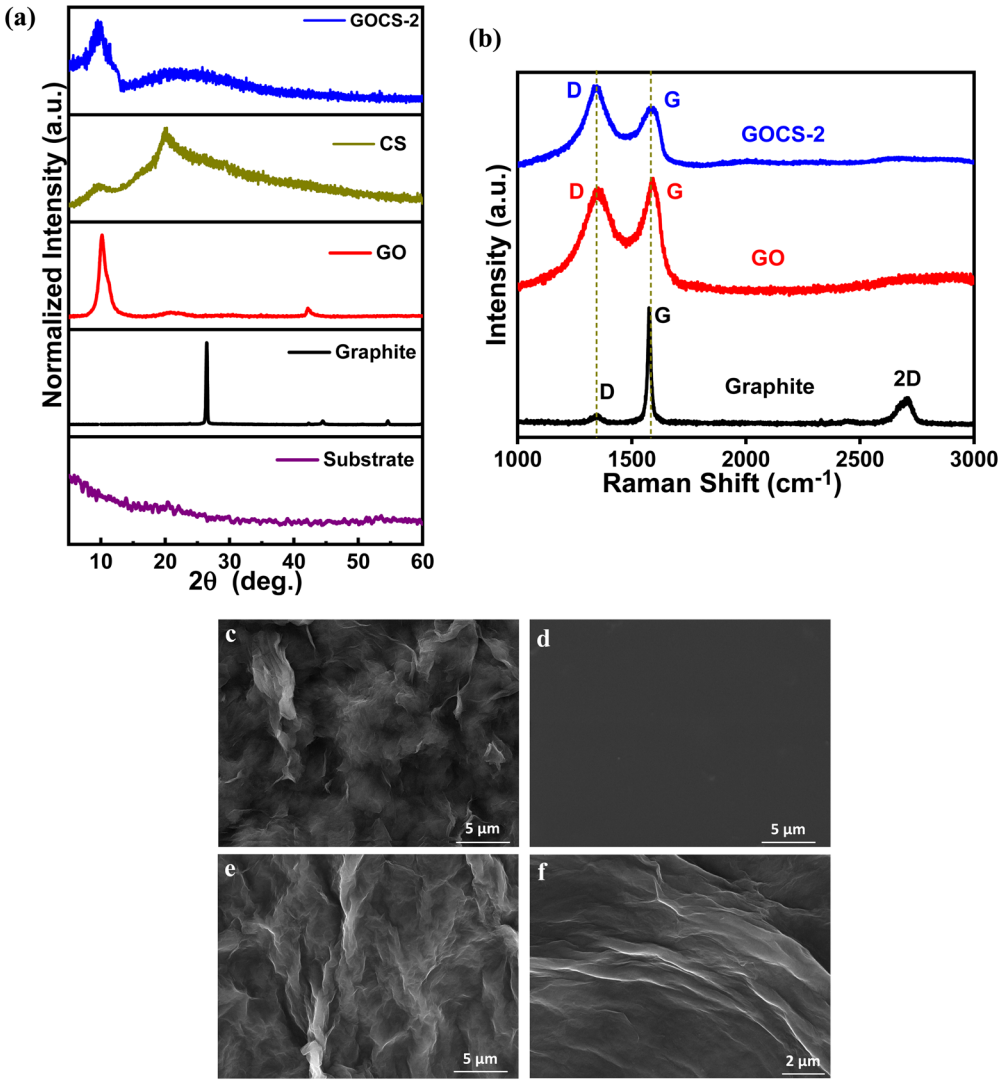

Fig. 2 (a) XRD of the substrate, graphite, GO, CS, and GOCS-2; (b) Raman spectra of graphite, GO, and GOCS-2; (c)–(f) SEM images of (c) GO, (d) CS (e) and (f) GOCS-2 at different magnifications.

(sp^2, 284.6 eV), C–O (epoxy/hydroxyls, 285.9 eV), and C═O (sp^3, 287.4 eV). The N1s spectra show peaks at 399.7 and 401.2 eV corresponding to N–H and NH_2 bonds (Fig. 3(c)). The appearance of an amide peak in the composite provides further evidence for the functionalization of CS on GO. Furthermore, the contact angle of each film was measured to understand the hydrophilic nature (Fig. 3(d)). The composite shows a water contact angle of 45.15°, which indicates optimal hydrophilicity, enhancing the adsorption of water molecules and improves the humidity sensor response.[34]

Sensing performance

The humidity sensing performance of all GO, CS, GOCS-1, GOCS-2, and GOCS-3 sensors was tested in the range of 11–95% RH at room temperature (Fig. 4(a)). All measurements were conducted by measuring the resistance with various humidity levels of each sensor. The composite based sensors exhibited high sensitivity over GO, attributed to the hydroxy and amine groups of CS, which provide ample water adsorption sites. Fig. 4(b) shows the sensitivity of GO, CS, and GO–CS composite based sensors, calculated according to eqn (1):

$$S\,(\%) = \left(\frac{R_{11} - R_{95}}{\mathrm{RH}_{11} - R_{95}}\right) \times 100 \quad \mathrm{in}\left(\frac{\Omega}{\%\mathrm{RH}}\right) \qquad (1)$$

The GO and CS have a sensitivity of 0.104 MΩ/%RH and 5.8 MΩ/%RH, respectively, whereas the GOCS-2 composite demonstrates a notable increase in sensitivity to 7.9 MΩ/%RH. The significant enhancement in sensitivity may be due to irregular arrangement of GO flakes and the strategic insertion of CS between GO layers in an optimal composition. However, once the ratio of GO is increased from 4 : 1 to 8 : 1, the GOCS-3 sample shows a reduction in performance.

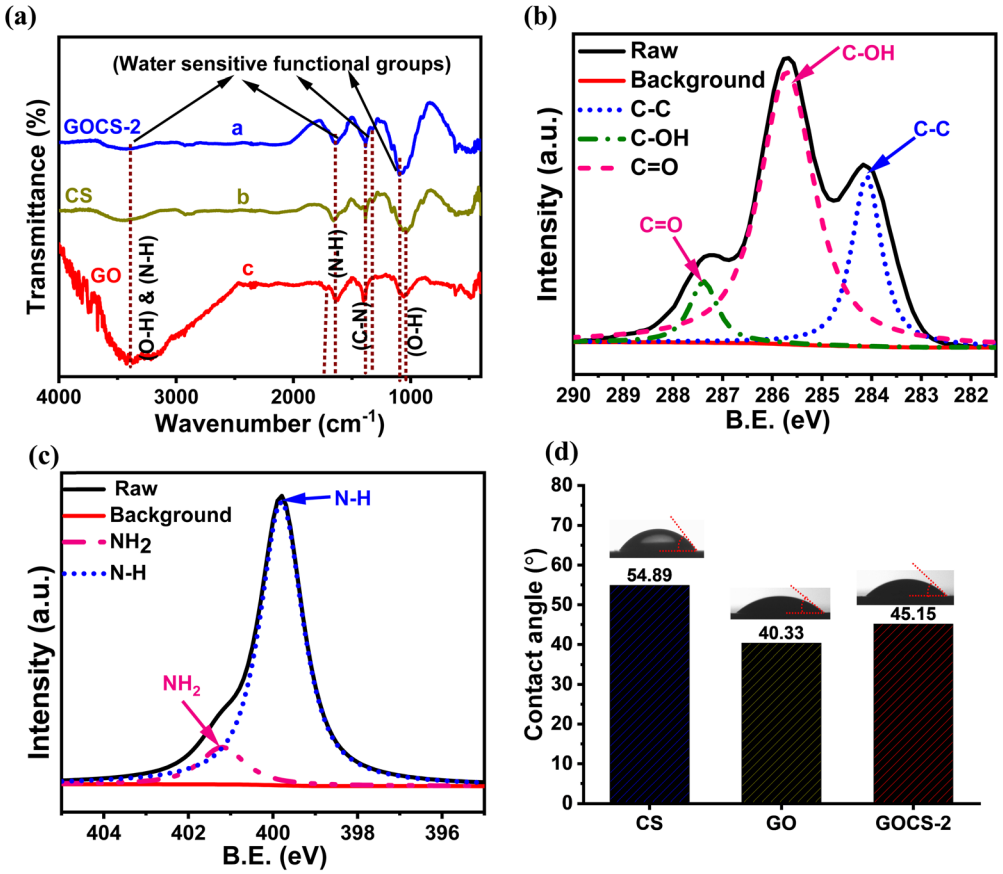

Fig. 3 (a) FTIR and (b) high resolution C1s spectra of the GOCS-2 composite; (c) high resolution N1s spectra of the GOCS-2 composite; (d) water contact angle measurement of GO, CS, and the GOCS-2 composite.

The transient response of the sensors was analyzed to calculate the response/recovery time during adsorption/desorption, defined as "the amount of time taken for the resistance change by 90% of the actual resistance value". The bars in Fig. 4(c) addressed the res/rec time of all the sensors and showed a quick res/rec time of 0.6/14 s for the GOCS-2 sensor. This significant result is attributed to the interlinking of CS and GO, which permits efficient charge transport and enables rapid response to humidity changes.

The hysteresis of each sensor was calculated by measuring the difference in resistance at a given RH level during humidification and dehumidification; the hysteresis values are summarised by the curves in Fig. 4(d). The maximum humidity hysteresis for the GOCS-2 composite was 2.9% under 33% RH (blue line), suggesting that hysteresis decreases with an increase in concentration of GO. Although the hysteresis of the GOCS-3 is shown to be lower when considering the overall performance, the GOCS-2 has a significantly larger response magnitude, and the narrow hysteresis loop in the composite sensors suggests that the processes of water adsorption and desorption are almost similar. Additionally, the efficient moisture diffusion properties of the GO–CS composite lead to rapid resistance changes, resulting in a fast response time and low hysteresis.

Fig. 5(a) illustrates a linear relationship in the $\log R$ *vs.* RH response curve, with a slope of 9.16 in the RH range from 11% to 95%. The response curve for the base materials and other compositions is shown in ESI,† Fig. S2. The high R^2 values of the fitted curve indicate an excellent fit, enhancing the linearity. Furthermore, to check the repeatability and long-term stability of the GOCS-2 sensor, the transient response is measured for multiple cycles at various RH, and the corresponding responses are shown in Fig. 5(b) and (c). The sensor shows remarkable repeatability towards different humidity sensing levels without experiencing any detectable degradation. The error bar graph for stability is shown in Fig. 5(d), which indicates that only a slight fluctuation is noticed in resistance up to 60 days, confirming the long-term stability of the sensor. Table 1 provides a comparative analysis of the humidity sensing performance of recently reported studies based on GO and other composites, offering a better understanding of the results.

Additionally, the accuracy and consistency measurements of the sensor are assessed through standard deviation and uncertainty calculations. The detailed mathematical expressions for standard deviation (σ) and standard uncertainty (S.U.) have been thoroughly discussed in our previous work.[29] In brief, the standard deviation quantifies the variability of data during repeated humidity measurements, while standard uncertainty defines the uncertainty associated with the average measured value. The standard deviation derived from five repeated measurements at each RH level and the associated uncertainty values along all RH ranges are given in Fig. 5(e). Thus, the maximum

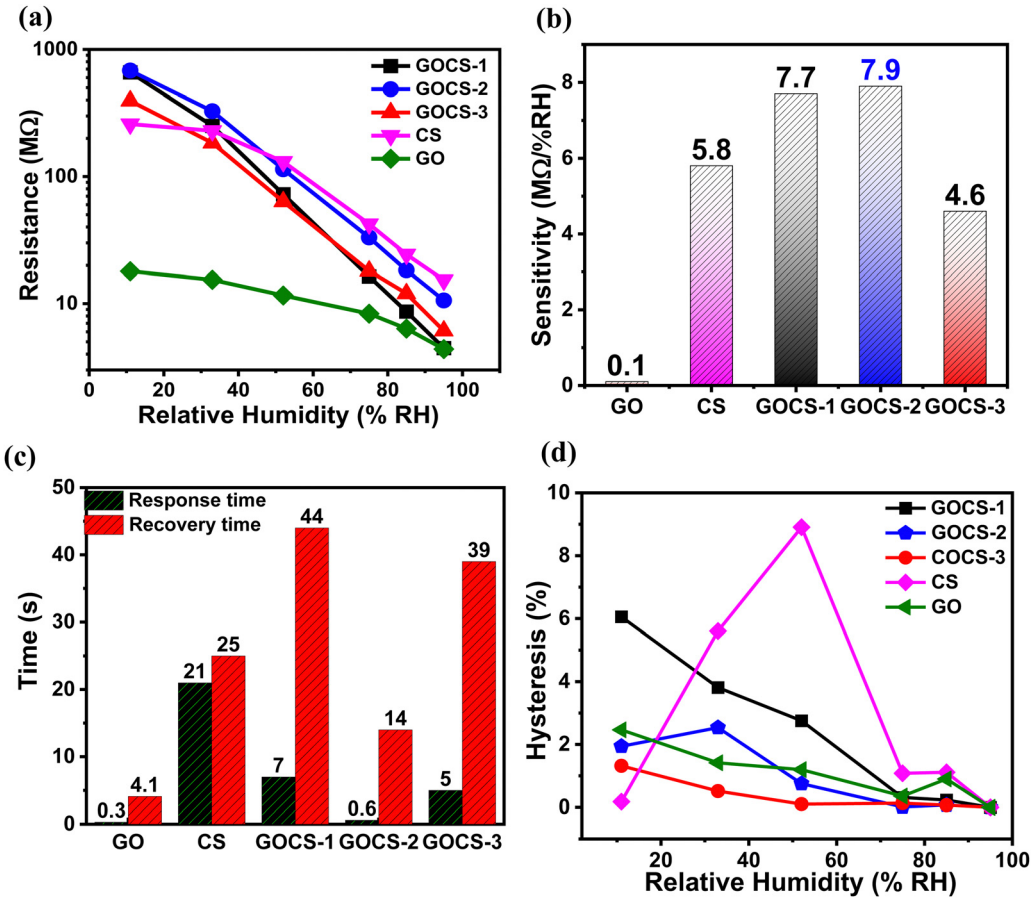

Fig. 4 (a) Logarithmic scale resistance response of the proposed sensor with relative humidity, (b) sensitivity of all fabricated samples, (c) response/recovery time of all samples and (d) hysteresis % values of all the samples.

standard uncertainty was found to be ±0.44 MΩ with standard deviation ±0.99 MΩ at 11% RH. The calculated standard uncertainty and standard deviation values across all measured humidity levels demonstrate excellent repeatability and reliable performance of the optimised sensor.

To check the sensor's capability to resist environmental influence, the sensor was exposed to other gas species present in the environment. Fig. 5(f) demonstrates that the GOCS-2 sensor exhibits minimal response to gases such as ethanol (C_2H_6O), ammonia (NH_3), formaldehyde (HCHO), acetone (C_3H_6O), carbon monoxide (CO), and hydrogen sulfide (H_2S) in comparison to its humidity response from 11–95% RH, which suggests the excellent anti-gas interference capability. The concentration of gases was maintained at 500 ppm, except for CO, which was tested at 40 ppm (for more information, see Supporting Note 1 in the ESI†). Overall, the GOCS-2 composite is revealed as efficient, stable, selective to water molecules, and a suitable candidate for humidity sensing applications.

The sensing mechanism of the fabricated humidity sensor (Fig. 6) relies on the adsorption of water molecules on the GO–CS composite film surface, which contains oxygenated functional groups. Being polar in nature, these functional groups are capable of adsorbing water molecules present in the environment through hydrogen bonding.[43] Hence, the sensor performance is based on change in resistance due to adsorption of water molecules.[33] The inclusion of CS increases hydrophilic functional groups and widens the interlayer spacing of GO layers in the composites, producing a synergistic effect that enhances surface active sites for water adsorption.[44]

At low RH, water molecules get strongly adsorbed onto the surface with hydrophilic functional groups of the film through hydrogen bonding, which resist their mobility, resulting in a high resistance value. With increase in RH, there is multilayer physisorption of water molecules through weak hydrogen bonding and some water molecules also penetrate into the GOCS layers and hydrolyse the carbonyl and hydroxyl groups, and the ions produced due to hydrolysis contribute to the ionic conductivity.[45–47]

Thus, the ions generated due to the ionization of adsorbed water molecules and hydrolysis of functional groups cause the increase in the ionic conductivity, which results in decreased resistance through the Grotthuss mechanism (eqn (2) and (3)), where water molecules react with an H^+ group to generate H_3O^+ ions, which subsequently undergo dissociation into H_2O and H^+ ions.

$$H^+ + H_2O \rightarrow H_3O^+ \quad (2)$$

$$H_3O^+ \rightarrow H_2O + H^+ \quad (3)$$

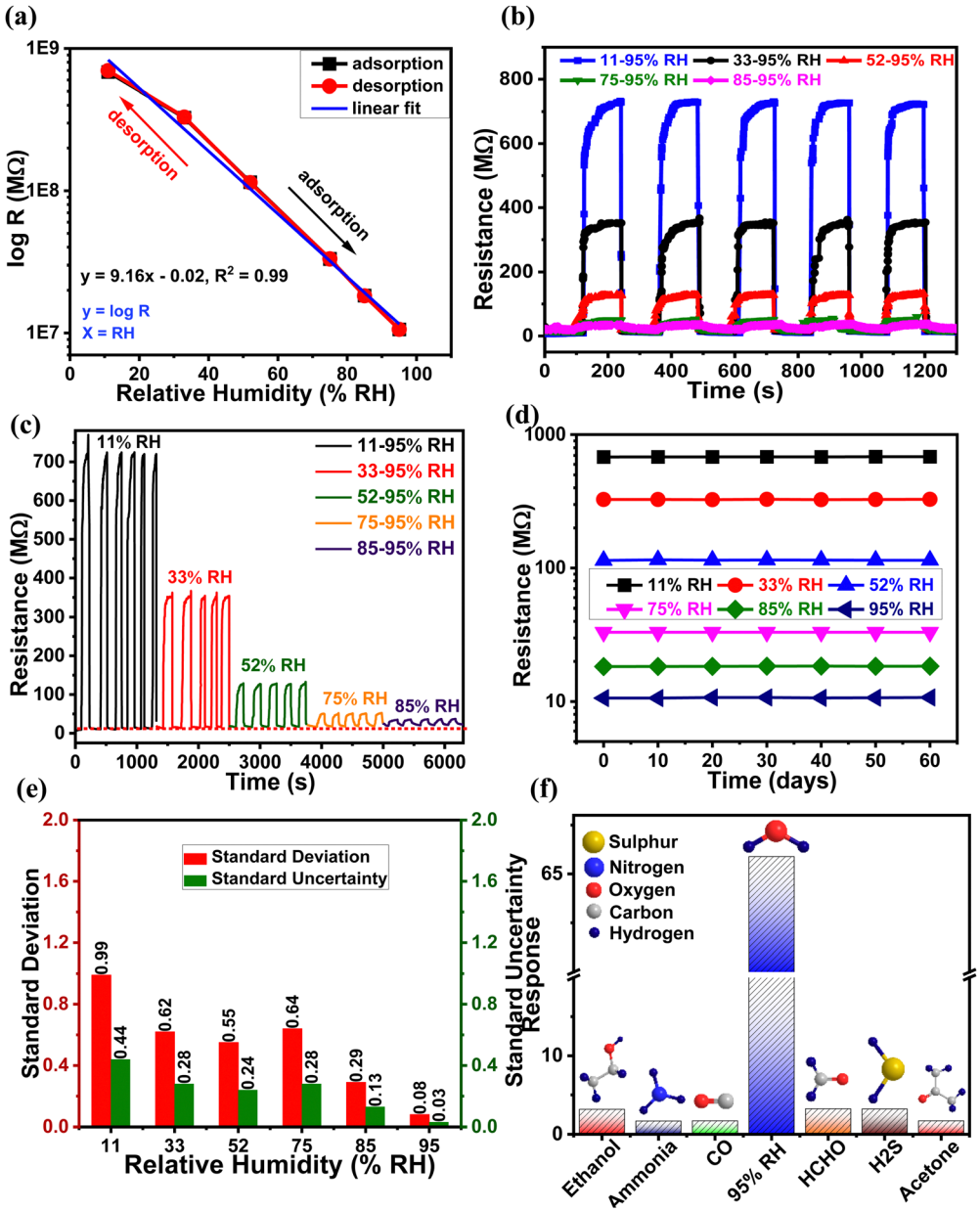

Fig. 5 (a) The transformed response curves of logarithmic resistance *vs.* RH, (b) response and recovery curves up to 5 cycles, (c) repeatability, (d) logarithmic scale humidity sensing stability, (e) standard deviation and standard uncertainty at different RH values and (f) selectivity of the GOCS-2 composite.

Table 1 Comparative analysis of the humidity sensing properties of previously reported sensors

	Material	Sensor type	Res/rec time	Response	Detection range	Ref.
1	rGO/PDDA	Resistive	—	8.69–37.43%	11–97%RH	35
2	GO	Capacitive	10.5 s/41 s	46.3 pF per %RH	15–95%RH	8
3	CS/GO/SnO2	Impeditive	8 s/8 s	72 683%, 402.5 kΩ per %RH	0–85%RH	36
4	Cu-BTC/GO	Resistive	—	6200%	11–85%RH	37
5	GrF/ZnO	Resistive	0.4 s/4 s	7.77 μA per RH%	15–86%RH	38
6	Keratin/GO	Capacitive	21 s/56 s	633.12 pF per %RH	16–92%RH	39
7	SnO_2/PANI	Resistive	26 s/30 s	0.22%/RH	5–95%RH	40
8	RGO/PVP	Resistive	2.8 s/3.5 s	—	7–97.3% RH	41
9	SnO_2/RGO	Capacitive	102 s/6 s	1604.8 pF per %RH	11–97% RH	42

This behaviour at different RH levels is consistent with findings from published research, indicating the formation of multilayer water adsorption participating as a key factor in the humidity sensing mechanism.[8,45]

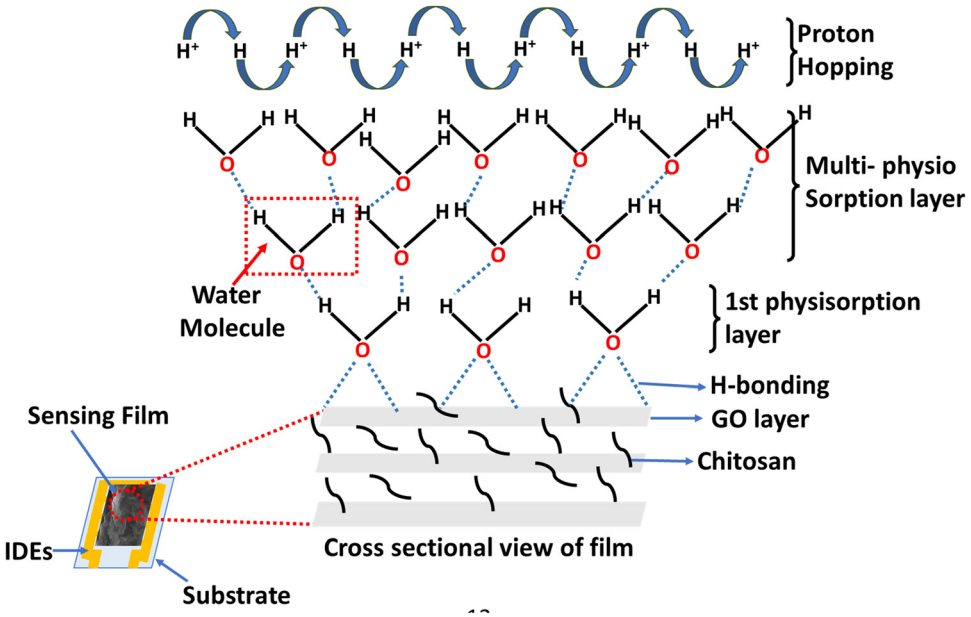

Fig. 6 Schematic diagram of the sensing mechanism of the film with water molecules, adapted with some modifications.[8]

4. Conclusion

In conclusion, we have studied the humidity sensing response of GO, CS and their composites (in different volumetric concentrations). Among all the synthesized composites, the GOCS-2 (4 : 1) composite reveals the best humidity sensing properties with a sensitivity of 7.9 MΩ/%RH, res/rec time of 0.6/14 s, low hysteresis of 2.9% at 33 %RH, and good repeatability, contrary to pure materials. The synergistic effect of CS as a support material in GO humidity sensors is also discussed. The fabricated sensor demonstrated robust and repeatable response to a broad operating range of humidity. The present study demonstrates the optimized composition of the GOCS composite as a high-performance humidity sensor.

Data availability

The data supporting this article have been included as part of the ESI.†

Conflicts of interest

There are no conflicts to declare.

Acknowledgements

The authors would like to thank Prof. Venu Gopal Achanta, Director, CSIR-NPL, and Head of Physico-Mechanical Metrology, for their constant support and encouragement. We acknowledge Dr Ajeet Kumar, Dr Nahar Singh, and Dr Govind Gupta for their help in depositing Ti/Au IDEs, GO synthesis, and gas sensing measurements. Mr Sumit, Dr Jai Tawale, Dr Vikas, Mr Rajat, and Mr Mukul are acknowledged for XRD, FESEM, water contact angle, Raman, and FTIR measurements. Our colleagues Dr Umesh Pant, Hansraj Meena, Gaurav Gupta, Ashish Bhatt, and Saroj Sharma from Temperature and Humidity Metrology are acknowledged for their help during this work. Ms Parvesh is grateful to UGC, India, for the financial support through the UGC–SRF fellowship and AcSIR India/RMIT Australia for a joint PhD program.

References

1 C.-Y. Lee and G.-B. Lee, Humidity Sensors: A Review, *Sens. Lett.*, 2005, **3**(1), 1–15, DOI: **10.1166/sl.2005.001**.
2 E. Traversa, Ceramic sensors for humidity detection: the state-of-the-art and future developments, *Sens. Actuators, B*, 1995, **23**(2–3), 135–156, DOI: **10.1016/0925-4005(94)01268-M**.
3 A. Kumar, G. Gupta, K. Bapna and D. D. Shivagan, Semiconductor-metal-oxide-based nano-composites for humidity sensing applications, *Mater. Res. Bull.*, 2023, **158**, 112053, DOI: **10.1016/j.materresbull.2022.112053**.
4 D. R. Dreyer, S. Park, C. W. Bielawski and R. S. Ruoff, The chemistry of graphene oxide, *Chem. Soc. Rev.*, 2010, **39**(1), 228–240, DOI: **10.1039/B917103G**.
5 S. J. Kim, H. J. Park, E. S. Yoon and B. G. Choi, Preparation of Reduced Graphene Oxide Sheets with Large Surface Area and Porous Structure for High-Sensitivity Humidity Sensor, *Chemosensors*, 2023, **11**(5), 276, DOI: **10.3390/chemosensors11050276**.
6 J. I. Paredes, S. Villar-Rodil, A. Martínez-Alonso and J. M. D. Tascón, Graphene Oxide Dispersions in Organic Solvents, *Langmuir*, 2008, **24**(19), 10560–10564, DOI: **10.1021/la801744a**.
7 J. Yang, *et al.*, Flame-retardant, flexible, and breathable smart humidity sensing fabrics based on hydrogels for respiratory monitoring and non-contact sensing, *View*, 2023, 20220060, DOI: **10.1002/VIW.20220060**.

8 H. Bi, *et al.*, Ultrahigh humidity sensitivity of graphene oxide, *Sci. Rep.*, 2013, **3**(1), 2714, DOI: **10.1038/srep02714**.
9 X. Li, X. Chen, X. Chen, X. Ding and X. Zhao, High-sensitive humidity sensor based on graphene oxide with evenly dispersed multiwalled carbon nanotubes, *Mater. Chem. Phys.*, 2018, **207**, 135–140, DOI: **10.1016/j.matchemphys.2017.12.033**.
10 D. Zhang, M. Wang and Z. Yang, Facile fabrication of graphene oxide/Nafion/indium oxide for humidity sensing with highly sensitive capacitance response, *Sens. Actuators, B*, 2019, **292**, 187–195, DOI: **10.1016/j.snb.2019.04.133**.
11 D. Zhang, X. Zong and Z. Wu, Fabrication of tin disulfide/graphene oxide nanoflower on flexible substrate for ultrasensitive humidity sensing with ultralow hysteresis and good reversibility, *Sens. Actuators, B*, 2019, **287**, 398–407, DOI: **10.1016/j.snb.2019.01.123**.
12 D. Zhang, Z. Xu, Z. Yang and X. Song, High-performance flexible self-powered tin disulfide nanoflowers/reduced graphene oxide nanohybrid-based humidity sensor driven by triboelectric nanogenerator, *Nano Energy*, 2020, **67**, 104251, DOI: **10.1016/j.nanoen.2019.104251**.
13 Q. Pan, T. Li and D. Zhang, Ammonia gas sensing properties and density functional theory investigation of coral-like Au–$SnSe_2$ Schottky junction, *Sens. Actuators, B*, 2021, **332**, 129440, DOI: **10.1016/j.snb.2021.129440**.
14 H. Zhang, D.-Z. Zhang, D.-Y. Wang, Z.-Y. Xu, Y. Yang and B. Zhang, Flexible single-electrode triboelectric nanogenerator with MWCNT/PDMS composite film for environmental energy harvesting and human motion monitoring, *Rare Met.*, 2022, **41**(9), 3117–3128, DOI: **10.1007/s12598-022-02031-z**.
15 D. Wang, D. Zhang, P. Li, Z. Yang, Q. Mi and L. Yu, Electrospinning of Flexible Poly(vinyl alcohol)/MXene Nanofiber-Based Humidity Sensor Self-Powered by Monolayer Molybdenum Diselenide Piezoelectric Nanogenerator, *Nano-Micro Lett.*, 2021, **13**(1), 57, DOI: **10.1007/s40820-020-00580-5**.
16 X. Liu, D. Zhang, D. Wang, T. Li, X. Song and Z. Kang, A humidity sensing and respiratory monitoring system constructed from quartz crystal microbalance sensors based on a chitosan/polypyrrole composite film, *J. Mater. Chem. A*, 2021, **9**(25), 14524–14533, DOI: **10.1039/D1TA02828F**.
17 J. Li, *et al.*, Improving Humidity Sensing of Black Phosphorus Nanosheets by Co-Doping Benzyl Viologen and Au Nanoparticles, *J. Electrochem. Soc.*, 2022, **169**(1), 017513, DOI: **10.1149/1945-7111/ac4b27**.
18 Y. Wang, *et al.*, Dual Resistance and Impedance Investigation: Ultrasensitive and Stable Humidity Detection of Molybdenum Disulfide Nanosheet-Polyethylene Oxide Hybrids, *ACS Appl. Mater. Interfaces*, 2021, **13**(21), 25250–25259, DOI: **10.1021/acsami.1c02119**.
19 R. Megha, Y. T. Ravikiran, B. Chethan, H. G. Raj Prakash, S. C. Vijaya Kumari and S. Thomas, Effect of mechanical mixing method of preparation of polyaniline-transition metal oxide composites on DC conductivity and humidity sensing response, *J. Mater. Sci.: Mater. Electron.*, 2018, **29**(9), 7253–7261, DOI: **10.1007/s10854-018-8714-z**.
20 S. Kotresh, Y. T. Ravikiran, H. G. Raj Prakash, Ch. V. V. Ramana, S. C. Vijayakumari and S. Thomas, Humidity sensing performance of spin coated polyaniline–carboxymethyl cellulose composite at room temperature, *Cellulose*, 2016, **23**(5), 3177–3186, DOI: **10.1007/s10570-016-1035-6**.
21 H. Dong, L.-X. Zhang, H. Xu, Y.-Y. Yin, Y.-F. Liu and L.-J. Bie, A highly efficient humidity sensor based on lead(II) coordination polymer via in-situ decarboxylation and hydrolysis synthesis, *Rare Met.*, 2022, **41**(5), 1652–1660, DOI: **10.1007/s12598-021-01913-y**.
22 N. Wang, X. Wang, Y. Jia, X. Li, J. Yu and B. Ding, Electrospun nanofibrous chitosan membranes modified with polyethyleneimine for formaldehyde detection, *Carbohydr. Polym.*, 2014, **108**, 192–199, DOI: **10.1016/j.carbpol.2014.02.088**.
23 H.-D. Wang, L.-Y. Chu, H. Song, J.-P. Yang, R. Xie and M. Yang, Preparation and enantiomer separation characteristics of chitosan/β-cyclodextrin composite membranes, *J. Membr. Sci.*, 2007, **297**(1–2), 262–270, DOI: **10.1016/j.memsci.2007.03.055**.
24 S. Moradi, H. Hamedi, A. E. Tonelli and M. W. King, Chitosan/Graphene Oxide Composite Films and Their Biomedical and Drug Delivery Applications: A Review, *Appl. Sci.*, 2021, **11**(17), 7776, DOI: **10.3390/app11177776**.
25 W. Li, D. M. Jang, S. Y. An, D. Kim, S.-K. Hong and H. Kim, Polyaniline–chitosan nanocomposite: High performance hydrogen sensor from new principle, *Sens. Actuators, B*, 2011, **160**(1), 1020–1025, DOI: **10.1016/j.snb.2011.09.020**.
26 E. Bagheripour, A. R. Moghadassi, S. M. Hosseini, B. Van Der Bruggen and F. Parvizian, Novel composite graphene oxide/chitosan nanoplates incorporated into PES based nanofiltration membrane: Chromium removal and antifouling enhancement, *J. Ind. Eng. Chem.*, 2018, **62**, 311–320, DOI: **10.1016/j.jiec.2018.01.009**.
27 W. S. Hummers and R. E. Offeman, Preparation of Graphitic Oxide, *J. Am. Chem. Soc.*, 1958, **80**(6), 1339, DOI: **10.1021/ja01539a017**.
28 Y. Chen, L. Chen, H. Bai and L. Li, Graphene oxide–chitosan composite hydrogels as broad-spectrum adsorbents for water purification, *J. Mater. Chem. A*, 2013, **1**(6), 1992–2001, DOI: **10.1039/C2TA00406B**.
29 P. Kumari, *et al.*, Chitosan-Based Highly Sensitive Viable Humidity Sensor for Human Health Monitoring, *ACS Omega*, 2023, **8**(42), 39511–39522, DOI: **10.1021/acsomega.3c05244**.
30 L. Shao, X. Chang, Y. Zhang, Y. Huang, Y. Yao and Z. Guo, Graphene oxide cross-linked chitosan nanocomposite membrane, *Appl. Surf. Sci.*, 2013, **280**, 989–992, DOI: **10.1016/j.apsusc.2013.04.112**.
31 A. Kumar, P. Kumari, M. S. Kumar, G. Gupta, D. D. Shivagan and K. Bapna, SnO_2 nanostructured thin film as humidity sensor and its application in breath monitoring, *Ceram. Int.*, 2023, **49**(15), 24911–24921, DOI: **10.1016/j.ceramint.2023.05.020**.
32 A. Yadav, Ultrahigh sensitive NO sensor based on WO_3 film with ppb-level sensitivity, *Ceram. Int.*, 2023, **49**, DOI: **10.1016/j.ceramint.2022.10.284**.
33 L. Liu, *et al.*, Preparation and characterization of chitosan/graphene oxide composites for the adsorption of Au(III) and Pd(II), *Talanta*, 2012, **93**, 350–357, DOI: **10.1016/j.talanta.2012.02.051**.

34 X. Feng, L. Feng, M. Jin, J. Zhai, L. Jiang and D. Zhu, Reversible Super-hydrophobicity to Super-hydrophilicity Transition of Aligned ZnO Nanorod Films, *J. Am. Chem. Soc.*, 2004, **126**(1), 62–63, DOI: **10.1021/ja038636o**.

35 D. Zhang, J. Tong and B. Xia, Humidity-sensing properties of chemically reduced graphene oxide/polymer nanocomposite film sensor based on layer-by-layer nano self-assembly, *Sens. Actuators, B*, 2014, **197**, 66–72, DOI: **10.1016/j.snb.2014.02.078**.

36 S. Wang, *et al.*, Fast response humidity sensor based on chitosan/graphene oxide/tin dioxide composite, *Sens. Actuators, B*, 2023, **392**, 134070, DOI: **10.1016/j.snb.2023.134070**.

37 W. Zhang, S. Meng, H. Wang and Y. He, Metal organic frameworks enhanced graphene oxide electrode for humidity sensor, *J. Phys.: Conf. Ser.*, 2018, **986**, 012013, DOI: **10.1088/1742-6596/986/1/012013**.

38 M. Saqib, *et al.*, High-Performance Humidity Sensor Based on the Graphene Flower/Zinc Oxide Composite, *Nanomaterials*, 2021, **11**(1), 242, DOI: **10.3390/nano11010242**.

39 H. Hammouche, H. Achour, S. Makhlouf, A. Chaouchi and M. Laghrouche, A comparative study of capacitive humidity sensor based on keratin film, keratin/graphene oxide, and keratin/carbon fibers, *Sens. Actuators, A*, 2021, **329**, 112805, DOI: **10.1016/j.sna.2021.112805**.

40 S. K. Shukla, S. K. Shukla, P. P. Govender and E. S. Agorku, A resistive type humidity sensor based on crystalline tin oxide nanoparticles encapsulated in polyaniline matrix, *Microchim. Acta*, 2016, **183**(2), 573–580, DOI: **10.1007/s00604-015-1678-2**.

41 Y. Su, *et al.*, Novel high-performance self-powered humidity detection enabled by triboelectric effect, *Sens. Actuators, B*, 2017, **251**, 144–152, DOI: **10.1016/j.snb.2017.04.039**.

42 D. Zhang, H. Chang, P. Li, R. Liu and Q. Xue, Fabrication and characterization of an ultrasensitive humidity sensor based on metal oxide/graphene hybrid nanocomposite, *Sens. Actuators, B*, 2016, **225**, 233–240, DOI: **10.1016/j.snb.2015.11.024**.

43 Y. Chen, L. Chen, H. Bai and L. Li, Graphene oxide–chitosan composite hydrogels as broad-spectrum adsorbents for water purification, *J. Mater. Chem. A*, 2013, **1**(6), 1992–2001, DOI: **10.1039/C2TA00406B**.

44 K. Zhang, R. Hu, G. Fan and G. Li, Graphene oxide/chitosan nanocomposite coated quartz crystal microbalance sensor for detection of amine vapors, *Sens. Actuators, B*, 2017, **243**, 721–730, DOI: **10.1016/j.snb.2016.12.063**.

45 K. Rathi and K. Pal, Impact of Doping on GO: Fast Response–Recovery Humidity Sensor, *ACS Omega*, 2017, **2**(3), 842–851, DOI: **10.1021/acsomega.6b00399**.

46 M. S. Siddiqui, V. S. Palaparthy, H. Kalita, M. S. Baghini and M. Aslam, Graphene Oxide Array for In-Depth Soil Moisture Sensing toward Optimized Irrigation, *ACS Appl. Electron. Mater.*, 2020, **2**(12), 4111–4121, DOI: **10.1021/acsaelm.0c00898**.

47 M. U. Khan, *et al.*, Wide range and highly linear signal processed systematic humidity sensor array using Methylene Blue and Graphene composite, *Sci. Rep.*, 2021, **11**(1), 16665, DOI: **10.1038/s41598-021-95977-6**.